Operando Determination of the Liquid-Solid Mass Transfer Coefficient During 1-Octene Hydrogenation

Qingyuan Zheng, Fernando J. Russo-Abegao[1], Andrew J. Sederman, Lynn F. Gladden*

University of Cambridge
Department of Chemical Engineering and Biotechnology
West Cambridge Site
Philippa Fawcett Drive
Cambridge CB3 0AS
United Kingdom

Submitted: 19 February 2017

Revised: 21 April 2017

* Corresponding author: Lynn F. Gladden lfg1@cam.ac.uk

[1] Present address:
Newcastle University, School of Chemical Engineering and Advanced Materials

Abstract

Spatially-resolved and unresolved magnetic resonance measurements are used in combination with a partial least squares regression (PLSR) method to measure chemical composition within catalyst pellets during the 1-octene hydrogenation reaction occurring in a fixed bed of 0.3 wt% Pd/Al_2O_3 catalyst pellets. The PLSR method is used to discriminate between chemical species within and external to the void space of the catalyst pellets. The spatially-resolved data show that the hydrogenation and isomerisation reactions are dominant in the upper and lower region of the reactor, respectively. The local intra-pellet compositions also show product accumulation inside catalyst pellets consistent with reaction occurring under conditions of mass transfer limitation. An average measure of the intra-pellet composition within the whole bed was then used to estimate the liquid-solid mass transfer coefficient during the course of the reaction. The values of k_{LS} obtained from the NMR measurements were in the range 0.15×10^{-5} m s^{-1} $< k_{LS} < 0.25 \times 10^{-5}$ m s^{-1}, for reactor operating conditions characterised by gas and liquid Reynolds numbers $0.2 < Re_L < 0.6$ and $0.1 < Re_G < 0.2$; these values are shown to be consistent with those predicted by existing literature correlations. Closest agreement was found with values predicted from dissolution experiments performed under similar hydrodynamic conditions in trickle flow. In addition to introducing a method for the direct measurement of k_{LS}, the data presented also confirm that estimates of k_{LS} are more accurate when performed in an environment in which the hydrodynamics and fluid-solid contacting conditions are representative of the system of interest.

Keywords: *operando* measurement, liquid-solid mass transfer, intra-pellet composition, ^{13}C DEPT NMR, PLSR

1. Introduction

In heterogeneous catalysis, understanding of the coupling of mass transport and reaction at the local pellet scale is central to our ability to design catalysts and operate catalytic processes effectively (Dudukovic et al., 1999; Dudukovic, 2010). The liquid-solid mass transfer is characterised by the liquid-solid mass transfer coefficient k_{LS}. Measurement of k_{LS} is not straightforward, with measurements being made outside the reactor (*ex situ*) on systems demonstrating liquid-solid mass transfer limitation, or on the working reactor (*in situ*) in which case k_{LS} is usually a parameter in the modelling of the reaction data. *Ex situ* methods have the advantage that they are easy to implement and can provide a direct measurement of k_{LS}. However, the obvious disadvantage is that the measurement is not taking place in the real reactor environment and in many cases will be taking place in systems in which the chemical species and hydrodynamic regimes differ from those found in the particular reaction of interest. Examples of *ex situ* methods include the dissolution method (Goto and Smith, 1975; Ruether et al., 1980; Sylvester and Pitayagulsarn, 1975), the electrochemical method (Burghardt et al., 1995; Chou et al., 1979; Rao and Drinkenburg, 1985), the ion exchange method (Yoshikawa et al., 1981) and the dynamic adsorption method (Tan and Smith, 1982). In the *in situ* approach, a correlation between k_{LS} and reactor operating properties such as liquid and gas flow velocities are usually assumed and the parameters of the correlation are then determined by regressing the reaction data onto the reactor model. Examples of the *in situ* approach include measurement of k_{LS} in the hydrogenation of α-methylstyrene (Morita and Smith, 1978), of styrene, 1-octene and toluene (Liu et al., 2005) and of linear and iso-octenes (Houwelingen and Nicol, 2011). Whilst k_{LS} is obtained under reaction conditions, this method relies on assumed reaction kinetics and the use of a correlation to define k_{LS}. Thus, the approach does not provide a direct measurement. In summary, a method that can provide a direct and non-invasive measurement of k_{LS} that is determined during operation of the catalyst in its working environment (i.e. under *operando* conditions) has not been reported. It is the purpose of this work to demonstrate a direct measurement of k_{LS} using magnetic resonance measurements of chemical composition within catalyst pellets (i.e. intra-pellet) made during 1-octene hydrogenation occurring in a fixed bed of 0.3 wt% Pd/Al_2O_3 catalyst pellets.

Tomographic and imaging methods, including capacitance and X-ray tomographies and magnetic resonance imaging (MRI) are increasingly applied to provide non-invasive and local measurements of multiphase reaction systems (Ranade et al., 2011). Of these, MRI is the only technique that can provide chemically-resolved information directly without need of any tracer or isotopic labels. MRI is now well-established as a technique for imaging hydrodynamics in fixed-bed reactors. These methods have been used to probe structure-flow correlations (Sederman et al., 1997) and local transitions in single-phase flow within packed beds (Johns et al., 2000); velocity imaging of both gas- and liquid-phase flow in a trickle bed (Sankey et al., 2009); and characterisation of the trickle-to-pulse hydrodynamic transition during trickle flow (Anadon et al., 2006), but the ability to track chemical conversion is less well-developed. Early applications of MRI to tracking reactions in heterogeneous catalytic reactors focussed on imaging of the ^{1}H nucleus (often referred to as proton MRI) and include esterification reactions (Kuppers et al., 2002; Yuen et al., 2002, 2003) and the hydrogenation of α-methylstyrene (Koptyug et al., 2004). Recently, a study of the gas phase ethylene hydrogenation reaction using ^{1}H NMR imaging has been reported by Ulpts et al. (2015). Whilst it is possible to spatially resolve the progress of reaction along the length of the reactor, accurate measurement of intra-pellet chemical composition has not been reported. This arises from two major measurement challenges in using ^{1}H MRI in this application. First, while MRI measurements of the ^{1}H nucleus are much favoured because of the high isotopic abundance of the ^{1}H nucleus and its high NMR sensitivity, it is associated with a narrow frequency range, termed the chemical-shift range, which means that it is difficult to unambiguously discriminate between different chemical species in a typical catalytic conversion. Second, the same chemical species will be present both inside and outside the catalyst pellets and one would therefore expect the magnetic resonance (MR) resonances to be indistinguishable for a given chemical species in the intra- and inter-pellet space. However, the interactions of a molecule within the confined pore space of the catalyst influence its nuclear spin-lattice (T_1) and spin-spin (T_2) relaxation times; the latter also acting to broaden the linewidth of the resonance. Thus, although it is challenging to distinguish the same species in the intra- and inter pellet space unambiguously it is, in principle, possible to do this and hence quantify intra-pellet composition during reaction. The first of these challenges was addressed by Akpa et al. (2005) who reported the application of ^{13}C MRI to spatially-resolve conversion and selectivity during the competing etherification and hydration reactions of 2-methyl-2-butene in a fixed-bed reactor. The ^{13}C nucleus has a chemical shift range of 200

ppm, compared to that of 10 ppm for ^{1}H observation. This approach was then used by Sederman et al. (2005) to obtain local compositions along the length of the reactor in a study of the hydrogenation of 1-octene in a trickle-bed reactor. In that work the use of ^{13}C observation enabled discrimination of 1-octene, octane and 2-octene isomers (the two isomers were not resolved). Thus it was possible to track the extent of hydrogenation isomerisation within the system which would not have been possible using ^{1}H observation. Identification of intra-pellet composition was not reported in that work. In both the work of Akpa et al. (2005) and Sederman et al. (2005) the pulse sequence that was implemented such that spatially resolved spectra were obtained was the ^{13}C Distortionless Enhancement by Polarisation Transfer (^{13}C DEPT) pulse sequence of Doddrell et al. (1982). More recently, Weber et al. (2011) reported a study of both intra- and inter-pellet species present during the esterification of acetic acid and ethanol in a fixed-bed reactor of ion-exchange resin using ^{13}C MRI. Discrimination of the intra- and inter-pellet species was achieved using chemically-specific diffusion coefficient measurements. While quantitative spatially-resolved concentration measurements were obtained for the inter-pellet space, only relative changes in concentration in the intra-pellet space were obtained because the microstructure of the gel resin was sensitive to the chemical composition of the liquid within it, which, in turn, influences the relaxation times of the liquid interacting with the resin making quantification challenging.

This paper uses the ^{13}C DEPT MRI method used previously by Sederman et al. (2005) and combines it with a multivariate calibration method known as partial least square regression (PLSR) (Geladi and Kowalski, 1986; Martens and Næs, 1989; Næs et al., 2002) to analyse the NMR spectra and hence to obtain intra-pellet compositions along the length of the reactor whilst the hydrogenation and isomerisation reactions of 1-octene are occurring. This ability to measure intra-pellet compositions also allows us to measure k_{LS} during reaction. The method reported in the present paper provides an *operando*, direct measurement of k_{LS}. The values of k_{LS} measured in the present study are then compared to the predictions of correlations previously reported in the literature.

2. Experimental

2.1 Materials and experimental setup

The catalyst, supplied by Johnson Matthey plc, was a 0.3 wt% Pd/Al_2O_3 trilobe, eggshell catalyst of diameter and length 1.2 mm and 5 ± 2 mm, respectively. The pellets have an equivalent diameter of $d_P = 3.7 \times 10^{-3}$ m. The metal was distributed in an eggshell layer of thickness of 0.5 mm. Nitrogen analysis gave a BET surface area and a BJH pore diameter of 100.6 $m^2\ g^{-1}$ and 16.2 nm, respectively. 1-octene (purity > 99%), obtained from Acros Organics, was used as the liquid feed. A 50:50 mol% H_2/N_2 gas mixture (BOC Special Gases) was used as the gas feed. Composition measurement at the entrance to and exit from the reactor were made by gas chromatography (GC) using an Agilent 7890A analyser with a non-polar HP-5 capillary column of 30 m length × 320 μm i.d., with a measurement accuracy of $\pm$ 0.1 mol%.

The experimental setup is presented in Fig. 1. Liquid is delivered to the rig from a feed vessel (1) of 1.2 L using a HPLC pump (2). Gas is delivered to the rig from pressurised gas cylinders, the flow rate being controlled by the needle valves (3) and measured by a rotameter (4). A glass reactor (5) of 25 mm i.d. and 25 cm length was used. The catalyst pellets were packed in the reactor to a height of 30 mm. Layers of θ-Al_2O_3 cylinders were loaded above and below the catalyst bed to enhance liquid-gas saturation and support the catalyst bed. The reactor was placed within the vertical bore of the NMR magnet (6) with the catalyst bed located in the centre of the radio frequency (r.f.) coil (i.e. the imaging region). The effluent from the reactor exit was sampled from a sampling port (7) located on the return line for composition measurement by GC. The reactor effluent was collected in the waste vessel (8). For the chemical reduction of the catalyst and during reaction experiments, the system was operated in downflow mode without recycle. Following completion of a reaction experiment, the system was operated in the upflow mode with recycle to saturate the catalyst pellets with the feed of the next reaction experiment.

2.2 Reaction experiments

Prior to the first reaction experiment, the catalyst bed was first reduced for 2 h under a flow of a 50/50 mol% H_2/N_2 gas mixture at a flow rate of 480 ml min^{-1}. The reaction was then performed under 7 different operating conditions, hereafter referred to as Reactions 1-7. The feed superficial velocities and compositions for these 7 reactions are given in Table 1. All experiments were performed at 21 ˚C and 1 atm. The liquid flow velocities were selected to give sufficient residence time to achieve a measurable conversion in a single pass through the reactor along the 5 cm field-of-view in the imaging experiments. Reactions 1-3 were operated with a feed 1-octene/H_2 ratio of 11/1 while Reactions 4–7 were operated with the feed 1-octene/H_2 ratio of 21/1. The two feed ratios were chosen such that the reaction experiments were operated under hydrogen-lean conditions to minimise the reaction heat and prevent hot spots occurring within the reactor. Reaction 7 was operated at higher liquid and gas superficial velocities to investigate the effect of external mass transfer resistance.

The reaction experiments were performed as follows. For the first reaction experiment (Reaction 1), the reactor was first flooded with 1-octene liquid to saturate the catalyst pellets by recycling 500 – 1000 ml 1-octene from the bottom of the reactor (upflow and recycle mode) with a flow rate of 10 ml min^{-1}. The composition of the effluent liquid from the top of the flooded reactor was measured by GC every 15 min and the reactor was considered to reach mass transfer equilibrium when the difference between two consecutive GC measurements was < 0.1 mol%. This mass transfer equilibrium process took ~45 min. The reactor was then switched to the downflow, non-recycle mode, and the 1-octene feed was delivered into the reactor with the liquid superficial velocity reported in Table 1. The 50/50 mol% H_2/N_2 gas mixture was delivered into the reactor concurrently with the liquid at the corresponding gas superficial velocity (Table 1). The composition of the effluent liquid from the bottom of the reactor was measured by GC and the reaction was considered to reach steady state when the difference between consecutive GC measurements was less than 0.1 mol%. GC analysis showed that only 1-octene, n-octane and *trans*- and *cis*-2-octene were produced during reaction. After reaching steady state, ^{13}C DEPT NMR spectra were recorded both spatially-unresolved and spatially-resolved along the length of the reactor. After completing the experiment for Reaction 1, the reactor was drained and the procedure repeated with the initial saturation of the bed with 1-octene

2.3 Magnetic resonance experiments

All magnetic resonance experiments were performed on a Bruker AV 400 spectrometer with a 9.4 T vertical magnet, equipped with a 3-axis gradient set providing a maximum gradient strength in all 3 directions of 1.46 T m^{-1}. A birdcage radiofrequency (r.f.) coil with a diameter of 38 mm was used and dual-tuned to 100.64 and 400.23 MHz for ^{1}H and ^{13}C, respectively. The pulse sequence used in all experiments including the PLSR calibration experiments was the ^{13}C DEPT pulse sequence (Doddrell et al., 1982) shown in Fig. 2. By applying only the ^{1}H and ^{13}C r.f. pulses, a single spatially-unresolved spectrum was acquired. Inclusion of the linearly-varying additional magnetic field gradient (G_{phase}), enables acquisition of the spatially-resolved ^{13}C DEPT spectra. For clarification, spatially-resolved ^{13}C DEPT NMR spectroscopy is often referred to as one-dimensional ^{13}C DEPT MRI. Hereafter, we will refer only to spatially-unresolved and spatially-resolved NMR spectroscopy.

Details of the ^{13}C DEPT pulse sequence implementation are as follows. The duration of the 90^{o} pulses for ^{1}H and ^{13}C, calibrated for each experiment, were approximately 85 μs and 100 μs, respectively. The echo time τ was 4.1 ms. The angle of the third ^{1}H pulse of the DEPT sequence was set as $\theta = 45^{o}$ and a J-coupling constant of 123 Hz for the aliphatic peaks was used. The decoupling was performed with the tppm20 decoupling sequence (Bennett et al., 1995). The ^{13}C DEPT spectra were acquired with a recycle time of 2 s and 512 scans. These parameters were used in all ^{13}C DEPT NMR measurements made. Composition analysis requires consideration of only the spectral resonances associated with the CH_2 and CH_3 groups which occur in the spectral (chemical shift) range 14 – 34 ppm relative to tetramethysilane (TMS). The data acquisition time for the spatially-unresolved data was 17 min.

Spatial resolution of the ^{13}C DEPT measurement (Akpa et al., 2005; Yeung and Swanson, 1989) along the length of the bed, was achieved using the same pulse parameters as used in the spatially-unresolved measurements but with the addition of a phase-encoding gradient (G_{phase}) of duration 0.4 ms, ramped to a maximum value of 3.44 G cm^{-1} in 16 steps. The gradient was applied along the axial direction of the catalyst bed with a field-of-view of 50

mm in this direction, yielding a spatial resolution of 3.1 mm. Therefore, in the ^{13}C DEPT spatially-resolved measurements, spectra were recorded from each of 16, immediately adjacent, transverse slices of thickness 3.1 mm along the length of the reactor. A complete spatially-resolved dataset was acquired with 64 scans and a recycle time of 2 s between scans. The data acquisition time for the spatially-resolved data was 34 min. A typical dataset is shown in Fig. 3; the data shown were recorded for Reaction 1.

Two sets of magnetic resonance data were acquired during reactor operation. The spatially-resolved ^{13}C DEPT NMR data revealed a switch from hydrogenation to isomerisation along the length of the bed and provided evidence that mass transfer limitation existed within the bed. The ^{13}C DEPT spectra acquired without spatial resolution, over the entire volume of the bed, were then acquired to provide an overall measurement of intra-pellet composition, with the best possible signal-to-noise (SNR), to be used in the estimation of the mass-transfer coefficient (Section 3.4).

Two-dimensional (2D) images of liquid distribution were also acquired within the fixed bed using a 2D RARE pulse sequence (Henning et al., 1986). These data were acquired to measure bed voidage, surface wetting and liquid holdup within the bed. Images were recorded in the direction perpendicular to the direction of superficial flow. Data were acquired in an array of 128 × 128 data points; given the field-of-view of 30 mm × 30 mm, this gave an in-plane spatial resolution of 234 μm × 234 μm. The image slice thickness was 1 mm. Images were acquired with a recycle time of 5 s, an echo time of 4 ms, 64 averages, and a RARE factor of 32 was used, giving a total data acquisition time of 21 min.

3. Data Analysis

3.1 Introduction to PLSR

PLSR is a multivariate calibration method that has been widely applied in analytical chemistry to analyse spectroscopic data (Grahn, 1991; Haaland and Thomas, 1988). In PLSR modelling, measurements **X** ($n \times m$, where n is the number of samples and m is the number of x variables) and responses **Y** ($n \times p$, where p is the number of y variables) are related through

finding the principal components (PCs) or latent variables of **X** and **Y** by maximising the covariance between the PCs of **X** and **Y** (Gowen et al., 2011; Wold et al., 2001). The general structure of a PLSR model is shown as follows:

$$\mathbf{X} = \mathbf{T}\mathbf{P}' + \mathbf{E} \tag{1}$$

$$\mathbf{Y} = \mathbf{T}\mathbf{Q} + \mathbf{F} \tag{2}$$

where **T** ($n \times b$, where b, $b \leq m$, is the number of the PCs of **X**) is the score matrix of **X**, **P** ($m \times b$) and **Q** ($b \times p$) are the loading matrices of **X** and **Y**, respectively, and **E** and **F** are the matrices of residual information. The estimation of new responses $\widehat{\mathbf{Y}}$ can then be calculated from new measurements $\mathbf{X}_{\mathrm{new}}$:

$$\widehat{\mathbf{Y}} = \mathbf{X}_{\mathrm{new}}\hat{\mathbf{b}} \tag{3}$$

where $\hat{\mathbf{b}}$ is the matrix of regression parameters and is related to the score and loading matrices shown in Eq. (1) and (2).

In the present study, the PLSR models are applied to calculate the chemical compositions or mole fractions of inter- and intra-pellet liquid from NMR spectral data. Therefore, the responses $\mathbf{Y}$ are the inter- and intra-pellet compositions and the measurements $\mathbf{X}$ are the spectral data of the liquid mixtures with the compositions in $\mathbf{Y}$. The columns of $\mathbf{Y}$ correspond to the species in the inter- and intra-pellet space and the columns of $\mathbf{X}$ correspond to the data points in the NMR spectra. Each row of $\mathbf{X}$ and $\mathbf{Y}$ corresponds to the spectrum and compositions of a calibration sample, respectively. The model calibration was implemented in MATLAB using the nonlinear iterative partial least squares (NIPALS) algorithm (Höskuldsso, 1988; Wold et al., 1984). The optimal numbers of PCs were determined using a method based on bias-variance analysis proposed by Gowen et al. (2011) which yielded the optimal PC numbers of 5 for the 3 species in the intra-pellet liquid. The performance of the PLSR models was tested using external testing samples and the prediction error was estimated in the form of a root mean square error of prediction ($RMSEP$):

$$RMSEP = \sqrt{\frac{1}{N}\sum_{i=1}^{N}(\hat{y}_i - y_i)^2} \quad (4)$$

where N is the number of testing samples and $\hat{y}_i$ is the model estimation of y_i which is the actual composition value.

3.2 Implementation of PLSR Analysis

In the present work, PLSR analysis was required to discriminate between intra- and inter-pellet species within the fixed bed. Model calibration was done with a calibration dataset which was representative of the chemical mixture characteristic of the reaction under study: namely 1-octene, n-octane and 2-octene isomers. For the purposes of this calibration, since the NMR spectra of *trans*- and *cis*-2-octene isomers are similar, they were treated as one species. The PLSR models were calibrated with samples whose compositions varied in the ranges of 6.2–99.3 mol%, 0.1–28.8 mol% and 0.4–93.7 mol% for 1-octene, 2-octene and n-octane, respectively. Nine calibration compositions were employed with the compositions having been based on a simplex-centroid design (Voinovich et al., 2009). For each composition, the spectral data associated with the inter- and intra-pellet liquid were obtained separately. The inter- and intra-pellet spectra of the 9 compositions were then combined to generate a calibration set based on a mixture-mixture design (Borges et al., 2007). Full details regarding construction of the calibration set from inter- and intra-pellet spectra and the implementation of PLSR applied in this work are reported in Zheng (2016). Specific considerations regarding the implementation of PLSR in this work are:

(i) Since the pore structure of the catalyst gives rise to a change in T_2 and T_2* of any liquid contained with it, which will then influence the acquired NMR signal intensity, it is required that the calibration samples reflect the physical and chemical environment in which the real reaction will occur. For this reason the calibration experiments were performed in the same trickle-bed reactor as that used in the reaction experiments. Since reaction must not occur, the liquid mixture for calibration was co-fed with N_2 as the gas phase. The liquid and gas superficial velocities were 1

mm s^{-1} and 15 mm s^{-1} respectively for these calibration experiments. It is essential that the NMR data acquisition parameters (i.e., pulse parameters and delay times) are the same in both the calibration experiments and the reaction experiments.

(ii) The aim of the PLSR analysis is to differentiate inter- and intra-pellet liquid compositions. Since the lineshapes of the inter- and intra-pellet liquid of a calibration sample will be different, an optimised PLSR model for each of the two physical environments is required. This was achieved by obtaining spectra of the bed during flow of liquid with the calibration compositions, and then draining the liquid from the bed. The remaining NMR signal was then associated with only intra-pellet liquid. Subtraction of this intra-pellet liquid spectrum from the original spectrum yielded the spectrum associated with inter-pellet liquid. Thus, calibration datasets for the inter- and intra-pellet liquid were obtained from which to develop the independent PLSR models.

(iii) Since the 1-octene hydrogenation is an exothermic reaction, the temperature of the catalyst bed during the reaction could be slightly higher than that in the calibration experiment. Temperature can change the relaxation time of the liquid-phase species but is not expected to influence the lineshape and relative intensities between different peaks of the NMR spectra, and is therefore not expected to influence the PLSR model performance. The PLSR models were tested using spectra acquired at a temperature of 20 ˚C different from the calibration experiment. The result showed that the $RMSEP$ mol % values for both the intra- and inter-pellet PLSR models remained the same to within experimental error, therefore confirming the negligible influence of temperature on the models.

Using the methodology outlined in Section 3.1, the values of $RMSEP$ for the compositions of intra-pellet species were 0.47, 1.06 and 1.40 mol% for 1-octene, 2-octene and n-octane, respectively, and for the compositions of inter-pellet species were 0.93, 5.60 and 1.42 mol% for 1-octene, 2-octene and n-octane, respectively. Thus, the PLSR models can predict the intra-pellet composition accurately with a prediction error < 1.5 mol%. The prediction errors for the inter-pellet compositions were higher but generally < 5 mol%, except for 2-octene.

3.3 PLSR spectral analysis of data acquired during reaction

In applying the PLSR model to the *operando* reactor data, it is important to note that while for both the calibration and reaction datasets the intra-pellet space was fully-liquid saturated, and therefore associated with NMR spectra of similar SNR (> 50), the signal associated with the inter-pellet space in the reaction experiments was considerably lower than that in the calibration experiments because of the significantly lower flow rates during reaction. In the case of the spatially-resolved spectra, SNR was ~20 times lower than that characterising the calibration datasets. It follows that the prediction errors for the inter-pellet compositions during reaction will increase due to this decreased SNR. For this reason, we did not apply the PLSR model to measure inter-pellet compositions, instead using it to estimate only the intra-pellet compositions. The NMR data were analysed and used as follows:

(a) The spatially-resolved NMR spectra were used to obtain intra-pellet compositions of 1-octene, 2-octenes and 1-octane along the length of the catalytic bed.

(b) The spatially-unresolved data were used to obtain average values of intra-pellet compositions of the three components within the catalytic bed. Combining this measurement of the intra-pellet composition of 1-octene with an average value of the inter-pellet composition of 1-octene along the bed, based on GC measurements, the concentration difference of 1-octene between the inter- and intra-pellet space was obtained, which was then used in the calculation of the mass transfer coefficient for this system (Section 3.4).

The analysis of the spatially-resolved and unresolved data followed the same approach. To reduce the influence of noise, baseline regions of the ^{13}C DEPT spectra characterised by a SNR < 5 were excluded from the calculation of intra-pellet compositions (Faber and Rajko, 2007). Figure 3 shows the 9 spatially-resolved magnetic resonance datasets acquired for Reaction 1 that were used in the PLSR analysis to obtain the intra-pellet compositions along the length of the reactor. Analysis was performed on the central 9 slices to avoid the effects of r.f. coil heterogeneity on the data analysis. The same analysis procedure was applied to the data acquired for Reactions 2–7, and for the spatially-unresolved (i.e., volume-averaged) spectrum acquired for each reaction.

3.4 Determination of the mass transfer coefficients

According to the film theory of mass transfer, the k_{LS} of 1-octene at the steady state is defined as (Cussler, 2009):

$$k_{\mathrm{LS}}a_{\mathrm{w}} = \frac{XF_{\mathrm{L}}}{C_0 - C_{\mathrm{S}}} \tag{5}$$

where $X = 1 - C_{\mathrm{out}}/C_{\mathrm{in}}$ is the conversion of 1-octene, F_{L} is the molar flow rate of 1-octene in the feed liquid, and C_0 and C_{S} [mol m^{-3}] are the average concentrations of 1-octene in bulk liquid and on the external catalyst surface, respectively. In this analysis the value of C_{S} is assigned to be the intra-pellet concentration of 1-octene (C_{intra}) as determined by the PLSR analysis of the spatially-unresolved NMR data. Since internal mass transfer limitations may exist, there could be a small concentration gradient in the eggshell layer of the catalyst. Therefore, C_{intra} could be an under-estimate of the true value of C_{S}. The bulk liquid concentration C_0 averaged over the catalyst bed was calculated by averaging the 1-octene concentrations at the inlet and outlet of the reactor which were measured by GC. Table 2 shows the inter- and intra-pellet compositions (mole fractions) determined by GC and NMR respectively, which were converted to concentrations for substitution into Eq. (5).

The external wetting surface area a_{w} was calculated as:

$$a_{\mathrm{W}} = \phi a V_{\mathrm{c}} \tag{6}$$

where ϕ is the wetting efficiency of the bed; a is the specific surface area of the bed, and V_{c} is the volume of the catalyst bed which was taken to be 1.47×10^{-5} m^3. The bed porosity, wetting efficiency and liquid holdup were calculated directly from the magnetic resonance images for each of Reactions 1–7; typical images are shown in Fig. 4. The bed porosity was obtained from the image of the flooded bed (Fig. 4 (a)) by calculating the ratio between the number of pixels associated with the void space and the cross section of the bed. The bed porosity was determined to be $\varepsilon_{\mathrm{b}} = 0.39 \pm 0.01$. The total external surface of the pellets was also identified from these images. The wetted surface was identified from an image acquired

while the bed was operated under trickle-flow conditions, as shown in Fig. 4 (b). The wetting efficiency was calculated as the ratio of the number of pixels associated with the wetted surface and the total external surface. The total liquid holdup, h_t, was also obtained from the image of the bed operated at the trickle flow condition by calculating the ratio between the pixel numbers associated with inter-pellet liquid and the cross section of the bed. The wetting efficiency and liquid holdup data are reported in Table 3. The specific surface area of a reactor of the same packing and inner diameter has previously been determined directly from a three-dimensional magnetic resonance image to be 1071 m^{-1} (Dunckley, 2008). Thus, all the parameters in Eq. (5) are determined experimentally, and k_{LS} was then calculated directly from these data.

4. Results

4.1 Reaction experiments

The conversions of 1-octene were calculated using the concentrations of 1-octene at the inlet and outlet of the reactor, as measured by GC, and are presented in Table 1. As expected, for a given feed composition, the conversion of 1-octene decreases with increasing liquid velocity as a result of the decrease in residence time. Further, the conversions observed for the 1-octene/H_2 ratio of 11 are significantly larger than that for the 1-octene/H_2 ratio of 21 consistent with the reaction rate having been reported to be proportional to the concentration of hydrogen in the feed (Battsengel et al., 2002; Reynders and Nicol, 2011).

Figure 5 (a)–(f) show the local intra-pellet compositions obtained for Reactions 1–6 obtained from the NMR data. It is observed that the compositions of the 1-octene, 2-octene and n-octane species show similar variation in all reaction experiments. At the entrance to the bed (i.e., at axial positions < 10 mm), the composition of n-octane is larger than that of 2-octene. The composition of n-octane within the pellets then decreases along the bed, while the composition of 2-octene increases. This is consistent with the feed composition being hydrogen lean; hydrogen is consumed in the hydrogenation reaction along the first 10 mm of the bed; further downstream the isomerisation reaction to 2-octenes dominate. It is believed that the isomerisation does not consume molecular hydrogen H_2 (Turkevich and Smith, 1948),

and that any hydrogen required by the isomerisation reaction is not necessarily from molecular H_2 but may be supplied by the hydroxyl groups on the support surface (Gerberich and Hall, 1966; Wells and Wilson, 1967) and the hydrogen in hydrocarbon molecules (Thomson and Webb, 1976). The composition of 1-octene generally remains stable or slightly decreases along the catalyst bed. Comparing the results for different feed 1-octene/H_2 ratios, the local intra-pellet compositions of 1-octene for reactions with 1-octene/H_2 = 11 (Reactions 1–3) are smaller than those for reactions with 1-octene/H_2 = 21 (Reactions 4–7). This is consistent with the larger conversions for the feed richer in hydrogen, as reported in Table 1.

The maximum theoretical mole fractions of n-octane produced for these two feed conditions, calculated by assuming that all the feed H_2 is consumed in the hydrogenation of 1-octene, are 0.09 and 0.05 for the 1-octene/H_2 feed molar ratios of 11 and 21, respectively. For all reactions shown in Fig. 5 at the entrance to the bed where hydrogenation dominates, the mole fractions of n-octane exceed the maximum theoretical mole fractions, providing evidence of the presence of a mass transfer resistance; i.e., the intrinsic reaction rate is larger than the mass transfer rate, and accumulation of products occurs inside the catalyst pellets.

4.2 Liquid-solid mass transfer

Table 2 shows the inter- and intra-pellet compositions of the 3 species within the bed; the data for 1-octene will be used to calculate the value of k_{LS} for this reaction. Figure 6 shows the difference between the inter- and intra-pellet concentrations of 1-octene $\Delta C = C_0 - C_{\mathrm{intra}}$ which is plotted against liquid superficial velocity u_{L}. As expected, the values of ΔC are higher for 1-octene/H_2 = 11 due to the higher conversions compared to those for 1-octene/H_2 = 21. Further, it is seen that for a given feed condition, variations in u_{L} in the range 0.036 – 0.1 mm s^{-1} cause a negligible change in the concentration gradient ΔC. However, ΔC was significantly reduced in Reaction 7 when u_{L} was increased to 0.68 mm s^{-1} for the 1-octene/H_2 = 21 feed, consistent with the reactor now being operated under conditions of external mass transfer limitation. This observation is also consistent with the relatively high value of XF_{L} for Reaction 7 reported in Table 1.

Table 4 reports the values of k_{LS} calculated from the experimental data reported in this work for all reactions studied, along with the values of k_{LS} predicted by 5 correlations using the flow conditions of the 7 reactions. These data are plotted in Fig. 7 as a function of liquid Reynolds number, Re_L ($Re_L = u_L \rho_L d_P / \mu_L$). Re_L is calculated using an equivalent diameter of the pellet, d_P, of 3.7×10^{-3} m; the density, ρ_L, and viscosity, μ_L, of pure 1-octene at 20 ˚C are taken as 714.9 kg m^{-3} and 4.69×10^{-4} kg m^{-1} s^{-1}, respectively (Frenkel et al., 1997); and the liquid superficial velocity reported in Table 1. Considering the values of k_{LS} calculated from the experimental data reported in the present work, it is seen that the values increase with increasing Re_L for a given 1-octene/H_2 ratio and that k_{LS} is larger for lower 1-octene/H_2 ratio at similar Re_L.

5. Discussion

The values of k_{LS} obtained directly from the NMR studies of Reactions 1-6 are considered first; these lie in the range $(0.15 – 0.25) \times 10^{-5}$ m^2 s^{-1}. From Fig. 7 and Table 4 it is seen that, for a given Re_L, the k_{LS} values are higher for the feed richer in hydrogen. Two possible explanations of this result exist in the literature. First, since the hydrogenation of 1-octene is an exothermic reaction (Bennett and Lewis, 1958; Ghosh and Perlmutter, 1963) and the rate of reaction increases with increasing concentration of hydrogen in the feed, the operating temperature of the feed richer in hydrogen is expected to be higher. Given that k_{LS} is proportional to the diffusivity D ($k_{LS} = D/\delta$ (Fogler, 2006)), a modest increase for reactions occurring for the 1-octene/H_2 =11 relative to 1-octene/H_2=21 is expected. Second, an increase of gas flow rate has also been reported to lead to enhanced k_{LS}as a result of changes in gas-liquid interaction (Lakota and Levec, 1990; Saroha, 2010; Sylvester and Pitayagulsarn, 1975). Possible factors causing an increase in mass transfer include a reduction the cross-sectional area for liquid flow, resulting in an increase in liquid superficial velocity as gas flow rate is increased, and an increase in gas flow causing turbulence and inducing radial momentum in the liquid phase. However, it has also been reported that the effect of gas flow on k_{LS} is not significant for a bed packed with small pellets (d_P < 5 mm) due to the stagnant liquid pockets between small pellets which have little interaction with gas flow (Goto et al., 1975; Rao and Drinkenburg, 1985). Given the low values of Re_L and the size of pellets used

in the present work it is therefore suggested that the observed increase in k_{LS} with hydrogen concentration in the feed is associated with an increase in bed temperature. The value of k_{LS} for Reaction 7 acquired for the higher liquid flow, Re_L=3.8 and Re_G=1.3 is 6.54 × 10^{-5} m s^{-1}. Since these data were acquired under conditions of external mass transfer limitation they will not be discussed further.

The values of k_{LS} determined from the NMR data for Reactions 1-6 are now compared with values predicted using 5 correlations that have been reported in the literature. They are summarised as follows.

Correlation A: $\phi Sh = 0.815 Re_L^{0.822} Sc^{1/3}$; 20 ˚C; 1.5 < Re_L < 196, 0 < Re_G < 433, 940 < Sc < 2114 (Satterfield et al., 1978). Method: Dissolution method; fixed bed, packed with 3×3–6×6 mm cylinders to a length l_b = 70 cm and operated under trickle-flow conditions.

Correlation B: $\phi Sh = 0.24 Re_L'^{0.75} Sc^{1/3}$, $Re_L' = Re/h_t$, 20 ˚C, 70 < Re_L' < 250, 11 < Re_G < 122, Sc = 1951 (Rao and Drinkenburg, 1985). Method: Electrochemical method; fixed bed packed with 3×3– 6×6 mm cylinders, with properties ε_b = 0.349–0.362, a = 638–1302 m^{-1}, l_b = 240 cm and operated under trickle-flow conditions.

Correlation C: $\varepsilon_b Sh = (1 + 0.003 Re_L \sqrt{Re_G})(0.765 Re_L^{0.18} + 0.365 Re_L^{0.614}) Sc^{1/3}$, 30 ˚C, 0.5 < Re_L < 50, 0 < Re_G < 12, Sc = 334.2 (Yoshikawa et al., 1981). Method: Ion-exchange reaction; fixed bed packed with 0.46 – 1.3 mm diameter spheres, with the bed properties of ε_b = 0.371, a = 2903–8204 m^{-1}, l_b = 0.27–0.54 cm and operated under trickle-flow conditions.

Correlation D: $\phi Sh = 4.25 Re_L^{0.48} Sc^{1/3}$, 25 ˚C, 0.88 < Re_L < 34.5, 0.1 < Re_G < 2.7, Sc = 974 (Tan and Smith, 1982). Method: Dynamic adsorption process within a fixed bed packed with 1.34–4.06 mm granular particles, with bed properties of ε_b = 0.37–0.47, a = 783–2820 m^{-1}, l_b = 2–3.3 cm and operated under trickle-flow conditions.

Correlation E: $\phi Sh = 0.266 Re_L^{1.147} Sc^{1/3}$, 20 ˚C, $Re_L \leq 20$, Re_G = 0, Sc = 1220–5400 (Satterfield et al., 1978; Specchia et al., 1978). Method: Dissolution method; fixed bed packed with 3×3– 6×6 mm cylinders, with bed properties of ε_b = 0.38, a = N/A, l_b = 9–15 cm and operated at the trickle-flow condition with no gas flow.

The calculation of correlations were carried out using the parameters presented in Tables 1 and 3 along with the equivalent pellet diameter d_P = 3.7 × 10^{-3} m and the bed porosity ε_b = 0.39. For completeness we note that the range of values of Re_L and Re_G in our experimental studies Reactions 1-6 are 0.2 < Re_L < 0.6 and 0.1< Re_G <0.2. The estimates of k_{LS} are summarized in Table 4 along with those obtained directly for the NMR data. It is seen that the k_{LS} values obtained from the NMR measurements are generally of the same magnitude as the estimations by *Correlations A-E.* However, *Correlation D* (Tan and Smith, 1982) gave values an order of magnitude larger than our experimental data and the predictions of the other correlations. We note that this correlation was based on a dynamic adsorption process.

With reference to Fig. 7 it is seen that *Correlations A* and *E* are in closest agreement with the values calculated from the NMR study. Both of these correlations were obtained from data recorded under trickle-flow conditions in a packed bed, using the dissolution method. The NMR data lie closest to the predictions of *Correlation E*, that correlation being obtained under conditions of trickle flow in which the values of Re_L and Re_G and are most similar to those in our experimental setup. *Correlations B* and *C* overestimate the experimentally-determined values; these correlations were obtained using an electrochemical method, which is likely to be characterised by significantly different hydrodynamic conditions to those in our work, and the ion exchange reaction occurring in a fixed bed, respectively. As well as being derived from data recorded under somewhat higher gas and liquids Reynolds numbers, the experimental setup for *Correlation C* was designed to address packings of small pellets, with spheres of diameters in the range 0.46-1.3 mm. When compared with the experimental data presented in this work, the predictions of *Correlation C* are consistent with values of k_{LS} increasing with decreasing packing pellet size, as a result of the reduction of the liquid film thickness, δ, characterising mass transfer (Goto and Smith, 1975; Saroha, 2010; Tan and Smith, 1982).

The data presented confirm the importance of making the determination of k_{LS} under the same hydrodynamic conditions as are present under reaction conditions; this includes not only the gas and liquids Reynolds number but also the rivulet flow pattern which will determine surface wetting characteristics of the pellets. This work also highlights the value of the *operando* NMR technique which can be applied directly in the fixed-bed environment and with the reaction of interest occurring within the bed.

6. Conclusion

This work presents an NMR study of the intra-pellet compositions and liquid-solid mass transfer during the hydrogenation and isomerisation reaction of 1-octene. The local intra-pellet compositions along the axial direction of the reactor were measured for the first time using NMR combined with a PLSR analysis method. The results indicated that hydrogenation and isomerisation reactions were dominant in the upper and lower regions of the reactor, respectively. The local intra-pellet compositions also revealed product accumulation inside catalyst pellets providing evidence of mass transfer limitation within the system.

Operando measurement of the liquid-solid mass transfer coefficients k_{LS} was achieved using spatially-unresolved measurements of intra-pellet chemical compositions. The values of k_{LS} calculated from the NMR data were shown to be in general agreement with those estimated by empirical correlations. Further, best agreement was found when the hydrodynamic conditions and fluid-solid contacting characteristics under which a given correlation was derived most closely matched our experimental set-up. The NMR method provides a direct measurement which can be made at the operating conditions under which the reaction is occurring. This approach provides a method by which catalyst pellets and operating conditions can be screened to characterise mass transfer behaviour and aid selection of materials and operating conditions. The approach can be applied to any heterogeneous catalytic system which can be studied using conventional NMR techniques.

Acknowledgements

We wish to thank the Qatar National Research Foundation for funding this work. We also thank Dr. D.J. Holland for useful discussions.

Nomenclature

a	specific surface area of the bed [m^{-1}]
a_w	external wetting surface area [m^2]
b	number of principal components
$\hat{\mathbf{b}}$	matrix of regression parameters
C_0	Inter-pellet 1-octene concentration [mol m^{-3}]
C_S	1-octene concentration on the external surface of catalyst pellets [mol m^{-3}]
$C_{in,out}$	1-octene concentration at the inlet and outlet of the reactor [mol m^{-3}]
C_{intra}	Intra-pellet 1-octene concentration [mol m^{-3}]
ΔC	Concentration difference between inter- and intra-pellet liquid [mol m^{-3}]
D	diffusivity of 1-octene [m^2 s^{-1}]
d_P	equivalent diameter of pellets [m]
F_L	liquid molar flow rate of 1-octene [mol s^{-1}]
G	volumetric gas flow rate [ml min^{-1}]
h_t	total liquid holdup [-]
k_{LS}	liquid-solid mass transfer coefficient [m s^{-1}]
L	volumetric liquid flow rate [ml min^{-1}]
l_b	length of the bed [cm]
m	number of x variables or spectral pixel number
n	number of samples
N	number of testing samples
p	number of y variables or components in a mixture
$Re_{L,G}$	$u_{L,G}\rho_{L,G}d_P/\mu_{L,G}$, liquid and gas Reynolds number [-]
Re'_L	Re/h_t, modified Reynolds number [-]
$RMSEP$	root mean square error of prediction
Sc	$\mu_L/(\rho_L D)$, liquid Schmidt number [-]
Sh	$k_{LS}d_P/D$, Sherwood number [-]
$u_{L,G}$	superficial velocities of liquid and gas [m s^{-1}]
V_c	volume of the catalyst bed [m^3]
X	conversion [-]
$\mathbf{X}$	matrix of spectra
$\mathbf{X}_{new}$	matrix of new spectral data
$\mathbf{Y}$	matrix of mixture compositions
y_i, $\hat{y}_i$	the actual and model prediction values of composition, respectively
ε_b	bed porosity [-]
ϕ	wetting efficiency [-]
$\rho_{L,G}$	densities of liquid and gas [kg m^{-3}]
δ	external film thickness [m]
$\mu_{L,G}$	viscosities of liquid and gas [kg m^{-1} s^{-1}]

References

Akpa, B.S., Mantle, M.D., Sederman, A.J., Gladden, L.F., 2005. *In situ* ^{13}C DEPT-MRI as a tool to spatially resolve chemical conversion and selectivity of a heterogeneous catalytic reaction occurring in a fixed-bed reactor. Chem. Commun. 2741–2743.

Anadon, L.D., Sederman, A.J., Gladden, L.F., 2006. Mechanism of the trickle-to-pulse transition in fixed-bed reactors. AIChE J. 52, 1522–1532.

Battsengel, B., Datsevich, L., Jess, A., 2002. Experimental and theoretical studies on hydrogenation in multiphase fixed-bed reactors. Chem. Eng. Technol. 25, 621–626.

Bennett, A.E., Rienstra, C.M., Auger, M., Lakshmi, K.V., Griffin, R.G., 1995. Heteronuclear decoupling in rotating solids. J. Chem. Phys. 103, 6951–6958.

Bennett, J.A.R., Lewis, J.B., 1958. Dissolution rates of solids in mercury and aqueous liquids: The development of a new type of rotating dissolution cell. AIChE J. 4, 418–422.

Borges, C.N., Bruns, R.E., Almeida, A.A., Scarminio, I.S., 2007. Mixture-mixture design for the fingerprint optimization of chromatographic mobile phases and extraction solutions for camellia sinensis. Anal. Chim. Acta 595, 28–37.

Burghardt, A., Bartelmus, G., Jaroszynski, M., Kolodziej, A., 1995. Hydrodynamics and mass transfer in a three-phase fixed-bed reactor with cocurrent gas-liquid downflow. Chem. Eng. J. 58, 83–99.

Chou, T.S., Worley, F.L., Luss, D., 1979. Local particle-liquid mass transfer fluctuations in mixed-phase cocurrent downflow through a fixed bed in the pulsing regime. Ind. Eng. Chem. Fundam. 18, 279–283.

Cussler, E.L., 2009. Diffusion: Mass transfer in fluid systems, 3rd ed. Cambridge University Press, New York.

Doddrell, D.M., Pegg, D.T., Bendall, M.R., 1982. Distortionless enhancement of NMR signals by polarization transfer. J. Magn. Reson. 48, 323–327.

Dudukovic, M.P., 2010. Reaction engineering: Status and future challenges. Chem. Eng. Sci. 65, 3–11.

Dudukovic, M.P., Larachi, F., Mills, P.L., 1999. Multiphase reactors - revisited. Chem. Eng. Sci. 54, 1975–1995.

Dunckley, C.P., 2008. Magnetic resonance chemical mapping of catalytic reactors. University of Cambridge, UK.

Faber, N.M., Rajko, R., 2007. How to avoid over-fitting in multivariate calibration – The conventional approach and an alternative. Anal. Chim. Acta. 595, 98-106.

Fogler, H.S., 2006. Elements of chemical reaction engineering, 4th ed. Pearson Education Inc., US.

Frenkel, M., Gadalla, N.M., Hall, K.R., Hong, X., Marsh, K.N., 1997. TRC Thermodynamic tables: Hydrocarbon, non-hydrocarbon. Thermodynamic Research Center, Texas A&M University System.

Geladi, P., Kowalski, B.R., 1986. Partial least-squares regression: A tutorial. Anal. Chim. Acta 185, 1–17.

Gerberich, H.R., Hall, W.K., 1966. Studies of the hydrogen held by solids. IX. The hydroxyl groups of alumina and silica-alumina as sites for the isomerization of butene. J. Catal. 5, 99–110.

Ghosh, D.N., Perlmutter, D.D., 1963. Effects of solute purity, temperature and surfactants on solid-liquid mass transfer. AIChE J. 9, 474–479.

Goto, S., Levec, J., Smith, J.M., 1975. Mass transfer in packed beds with two-phase flow. Ind. Eng. Chem. Process Des. Dev. 14, 473–478.

Goto, S., Smith, J.M., 1975. Trickle-bed reactor performance Part I. AIChE J. 21, 706–713.

Gowen, A.A., Downey, G., Esquerre, C., O'Donnell, C.P., 2011. Preventing over-fitting in PLS calibration models of near-infrared (NIR) spectroscopy data using regression coefficients. J. Chemom. 25, 375–381.

Grahn, H., 1991. Multivariate data analysis of NMR data. J. Pharm. Biomed. Anal. 9, 655–658.

Haaland, D.M., Thomas, E. V., 1988. Partial least-squares methods for spectral analyses. 1 . Relation to other quantitative calibration methods and the extraction of qualitative information. Anal. Chem. 60, 1193–1202.

Hennig, J., Nauerth, A., Friedburg, H., 1986. RARE imaging – A fast imaging method for clinical MR. Magn. Reson. Med. 3, 823-833.

Hirschfelder, J.O., Bird, R.B., Spotz, E.L., 1948. The transport properties for non-polar gases. J. Chem. Phys. 16, 968–981.

Höskuldsso, A., 1988. PLS regression methods. J. Chemom. 2, 211–228.

Houwelingen, A.J.V., Nicol, W., 2011. Parallel hydrogenation for the quantification of wetting efficiency and liquid–solid mass transfer in a trickle-bed reactor. AIChE J. 57, 1310–1319.

Johns, M.L., Sederman, A.J., Bramley, A.S., Gladden, L.F., Alexander, P., 2000. Local transitions in flow phenomena through packed beds identified by MRI. AIChE J 46, 2151-2161.

Koptyug, I.V., Lysova, A.A., Kulikov, A.V., Kirillov, V.A., Parmon, V.N., Sagdeev, R.Z., 2004. Functional imaging and NMR spectroscopy of an operating gas–liquid–solid catalytic reactor. Appl. Catal. A267, 143–148.

Kuppers, M., Heine, C., Han, S., Stapf, S., Blumich, B., 2002. *In situ* observation of diffusion and reaction dynamics in gel microreactors by chemically resolved NMR microscopy. Appl. Magn. Reson. 22, 235–246.

Lakota, A., Levec, J., 1990. Solid-liquid mass transfer in packed beds with cocurrent downward two-phase flow. AIChE J. 36, 1444–1448.

Liu, W., Roy, S., Fu, X., 2005. Gas-liquid catalytic hydrogenation reaction in small catalyst channel. AIChE J. 51, 2285–2297.

Martens, H., Næs, T., 1989. Multivariate calibration. Wiley, Chichester, UK.

Morita, S., Smith, J.M., 1978. Mass transfer and contacting efficiency in a trickle-bed reactor. Ind. Eng. Chem. Fundam. 17 (2), 113–120.

Næs, T., Isaksson, T., Fearn, T., Davies, T., 2002. A user-friendly guide to multivariate calibration and classification. NIR Publications, Chichester, Uk.

Ranade, V.V., Chaudhari, R.V., Gunjal, P.R., 2011. Trickle bed reactors: Reactor engineering and applications. Elsevier, Oxford.

Rao, V.G., Drinkenburg, A.A.H., 1985. Solid-liquid mass transfer in packed beds with cocurrent gas-liquid downflow. AIChE J. 31, 1059–1068.

Reynders, F., Nicol, W., 2011. Gas-limited hydrogenation of 1-octene in a fixed bed: Upflow versus downflow. Ind. Eng. Chem. Res. 50, 10476–10479.

Ruether, J.A., Yang, C., Hayduk, W., 1980. Particle mass transfer during cocurrent downward gas-liquid flow in packed beds. Ind. Eng. Chem. Process Des. Dev. 19, 103–107.

Sankey, M.H., Holland, D.J., Sederman, A.J., Gladden, L.F., 2009. Magnetc resoance velocity imaging of liquid and gas two-phase flow in packed beds. J. Magn. Reson. 196, 142-148.

Saroha, A.K., 2010. Solid-liquid mass transfer studies in trickle bed reactors. Chem. Eng. Res. Des. 88, 744–747.

Satterfield, C.N., Van Eek, M.W., Bliss, G.S., 1978. Liquid-solid mass transfer in packed beds with downward concurrent gas-liquid flow. AIChE J. 24 (4), 709–717.

Sederman A.J., Johns, M.L., Bramley, A.S., Alexander P., Gladden, L.F., 1997. Magnetic resonance imaging of liquid flow and pore structure within packed beds. Chem. Eng. Sci. 52, 2239-2250.

Sederman, A.J., Mantle, M.D., Dunckley, C.P., Huang, Z., Gladden, L.F., 2005. *In situ* MRI study of 1-octene isomerisation and hydrogenation within a trickle-bed reactor. Catal. Letters 103, 1–8.

Specchia, V., Baldi, G., Gianetto, A., 1978. Solid-liquid mass transfer in concurrent two-phase flow through packed beds. Ind. Eng. Chem. Res. 17, 362-367.

Sylvester, N.D., Pitayagulsarn, P., 1975. Mass transfer for two-phase cocurrent downflow in a packed bed. Ind. Eng. Chem. Process Des. Dev. 14, 421–426.

Tan, C.S., Smith, J.M., 1982. A dynamic method for liquid-particle mass transfer in trickle beds. AIChE J. 28, 190–195.

Thomson, S.J., Webb, G., 1976. Catalytic hydrogenation of olefins on metals: A new interpretation. J. Chem. Soc. Chem. Commun., 526–527.

Turkevich, J., Smith, R.K., 1948. Catalytic isomerization of 1-butene to 2-butene. J. Chem. Phys. 16, 466–480.

Ulpts, J., Dreher, W., Klink, M., Thoming, J., 2015. NMR imaging of gas phase hydrogenation in a packed bed flow reactor. Appl. Catal. A Gen. 502, 340–349.

Voinovich, D., Campisi, B., Phan-Tan-Luu, R., 2009. Experimental design for mixture studies, in: Brown, S.D., Tauler, R., Walczak, B. (Eds.), Comprehensive chemometrics. Elsevier, Oxford, pp. 391-452.

Weber, D., Holland, D.J., Gladden, L.F., 2011. Spatially and chemically resolved measurement of intra- and inter-particle molecular diffusion in a fixed-bed reactor. Appl. Catal. A392, 192–198.

Wells, P.B., Wilson, G.R., 1967. Butene isomerization catalyzed by supported metals in the absence of molecular hydrogen. J. Catal. 9, 70–75.

Wilke, C.R., 1950. A viscosity equation for gas mixtures. J. Chem. Phys. 18, 517–519.

Wold, S., Albano, C., Dunn, W.J., Edlund, U., Esbensen, K., Geladi, P., Hellberg, S., Johansson, E., Lindberg, W., Sjöström, M., 1984. Multivariate data analysis in chemistry. in: Kowalski, B.R. (Ed.), Chemometrics: Mathematics and statistics in chemistry. Reidel Publishing Company, Dordrecht, pp. 17–95.

Wold, S., Sjostrom, M., Eriksson, L., 2001. PLS-regression : A basic tool of chemometrics. Chemom. Intell. Lab. Syst. 58, 109–130.

Yeung, H.N., Swanson, S.D., 1989. Imaging and localized spectroscopy of ^{13}C by polarization transfer. J. Magn. Reson. 83, 183–189.

Yoshikawa, M., Iwai, K., Goto, S., Teshima, H., 1981. Liquid-solid mass transfer in gas-liquid corurrent flows through beds of small packings. J. Chem. Eng. Japan 14, 444–450.

Yuen, E.H.L., Sederman, A.J., Gladden, L.F., 2002. *In situ* magnetic resonance visualisation of the spatial variation of catalytic conversion within a fixed-bed reactor. Appl. Catal. A Gen. 232, 29–38.

Yuen, E.H.L., Sederman, A.J., Sani, F., Alexander, P., Gladden, L.F., 2003. Correlations between local conversion and hydrodynamics in a 3-D fixed-bed esterification process: An MRI and lattice-Boltzmann study. Chem. Eng. Sci. 58, 613–619.

Zheng, Q., 2016. Magnetic resonance studies of intra-particle phenomena in porous media. University of Cambridge, U.K.

Tables

Table 1 Reaction conditions and conversion for the 1-octene hydrogenation experiments.

reaction	superficial velocity [mm s^{-1}]		feed molar ratio 1-octene/H_2	conversion of 1-octene X	XF_L [10^{-5} mol s^{-1}]
	liquid (u_L)	gas (u_G)			
1	0.036	1.0	11/1	0.120	1.35
2	0.052	1.5	11/1	0.095	1.53
3	0.070	2.0	11/1	0.107	2.30
4	0.050	0.71	21/1	0.051	0.787
5	0.073	1.0	21/1	0.040	0.904
6	0.10	1.5	21/1	0.043	1.38
7	0.68	9.7	21/1	0.036	7.62

Table 2 Average inter- and intra-pellet compositions (mole fractions) of Reactions 1–7 used in calculation of k_{LS}. The inter-pellet compositions were calculated by averaging the inlet and outlet compositions for each species as measured by GC. The intra-pellet compositions were determined from the PLSR analysis of the spatially-unresolved NMR spectra acquired from the whole catalyst bed.

reaction	inter-pellet composition [-]			intra-pellet composition [-]		
	1-octene	2-octene	n-octane	1-octene	2-octene	n-octane
1	0.930	0.055	0.015	0.716	0.234	0.050
2	0.941	0.043	0.016	0.724	0.222	0.054
3	0.937	0.048	0.015	0.718	0.225	0.057
4	0.968	0.022	0.010	0.841	0.132	0.027
5	0.975	0.015	0.010	0.843	0.125	0.032
6	0.973	0.016	0.011	0.844	0.111	0.045
7	0.980	0.014	0.006	0.955	0.041	0.004

Table 3 MRI measurements of the wetting efficiencies and total liquid holdups Reactions 1-7. Typical errors of the measured wetting efficiency and total liquid holdup are 0.01 and 0.005, respectively.

reaction	wetting efficiency ϕ	total liquid holdup h_t
1	0.41	0.078
2	0.41	0.077
3	0.43	0.083
4	0.42	0.080
5	0.42	0.081
6	0.42	0.081
7	0.47	0.089

Table 4 Values of k_{LS} measured by the NMR method and estimated using correlations taken from the literature, as discussed in the text. Values used in the calculation of k_{LS}, in addition to those already given, for calculation of Re_L are (i) the self diffusivity, *D*, of 1-octene measured by pulsed-field-gradient NMR at 20 ˚C = 2.88×10^{-9} m^2 s^{-1}; (ii) the liquid Schmidt number, *Sc* = 227.8 at 20 ˚C ; (iii) gas density, $\rho_{G,}$ = 0.62 kg m^{-3} calculated for 20 ˚C based on the ideal gas assumption; (iv) gas viscosity, μ_G = 1.7×10^{-5} kg m^{-1} s^{-1}, calculated using the correlation of Wilke (1950), with the viscosity of pure H_2 and N_2 at 20 ˚C calculated by the method of Hirschfelder et al. (1948).

	k_{LS} [10^{-5} m s^{-1}] in reaction						
	1	2	3	4	5	6	7
This work	0.15	0.17	0.24	0.15	0.16	0.25	6.54
Correlation A	0.26	0.34	0.42	0.32	0.45	0.60	2.49
Correlation B	0.57	0.76	0.85	0.69	0.92	1.20	4.08
Correlation C	0.87	0.96	1.04	0.95	1.05	1.17	2.23
Correlation D	2.30	2.73	3.00	2.61	3.14	3.73	8.19
Correlation E	0.05	0.08	0.10	0.07	0.11	0.16	1.26

Figure Captions

Figure 1: Schematic of the reactor rig. 1. Liquid feed vessel. 2. High pressure liquid chromatography (HPLC) pump. 3. Needle valve. 4. Rotameter. 5. Reactor. 6. NMR magnet. 7. Sampling port. 8. Waste vessel.

Figure 2: The ^{13}C DEPT pulse sequence. Implementation of the two r.f. excitations gives a spatially-unresolved NMR spectrum. By adding the additional magnetic field gradient along the direction of superficial flow (G_{phase}), spatial resolution of the NMR spectrum is achieved.

Figure 3: ^{13}C DEPT NMR spectra spatially resolved along the length of the reactor. The axial positions are identified at the mid-point of the image slice from which they were recorded. Each image slice had a thickness of 3.1 mm. Data are shown for Reaction 1.

Figure 4: 2D ^{1}H MRI data from which bed porosity, liquid holdup and wetting efficiency were calculated. Images are shown for a transverse slice section through the reactor: (a) the bed is flooded with liquid 1-octene, and (b) during Reaction 7. Both images have a field-of-view of 30 mm × 30 mm and were normalised to the maximum intensity in (a).

Figure 5: Intra-pellet compositions along the length of the catalyst bed, obtained from the spatially-resolved NMR data analysed using the PLSR models. (a)–(c) present the results of Reactions 1–3 with 1-octene/H_2 = 11, while (d)–(f) show the results of Reactions 4–6 with 1-octene/H_2 = 21. ● = 1-octene, ■ = 2-octene, ▲ = n-octane. The data for Reaction 7 are not shown because the intra-pellet concentrations of products were significantly lower than the other reactions due to the low conversion of this reaction (see Table 2).

Figure 6: Concentration difference between inter- and intra-pellet liquid in the 7 reaction experiments.

Figure 7: The $\boldsymbol{k_{LS}}$ measured by NMR and predicted by *Correlations A-E* plotted against liquid Reynolds numbers $\boldsymbol{Re_L}$. ● = NMR 1-octene/H_2 of 11, ■ = NMR 1-octene/H_2 of 21. Symbols □, ○, ▽, △ represent the results of *Correlations A*, *B*, *C* and *E*, respectively.

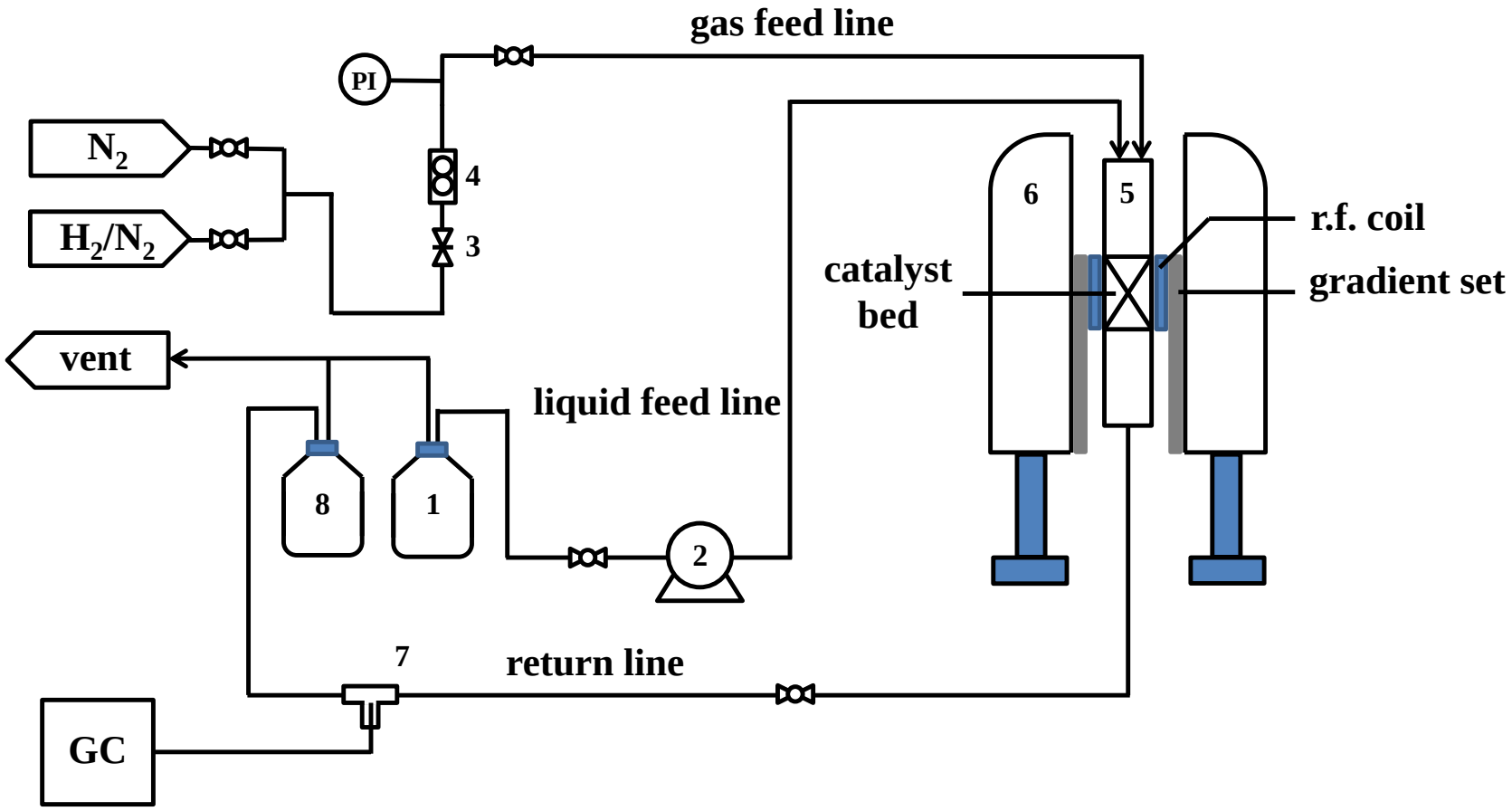
gas feed line
PI
N_2
H_2/N_2
4
3
vent
liquid feed line
8
1
2
7
return line
GC
6
5
r.f. coil
catalyst bed
gradient set

Figure 1

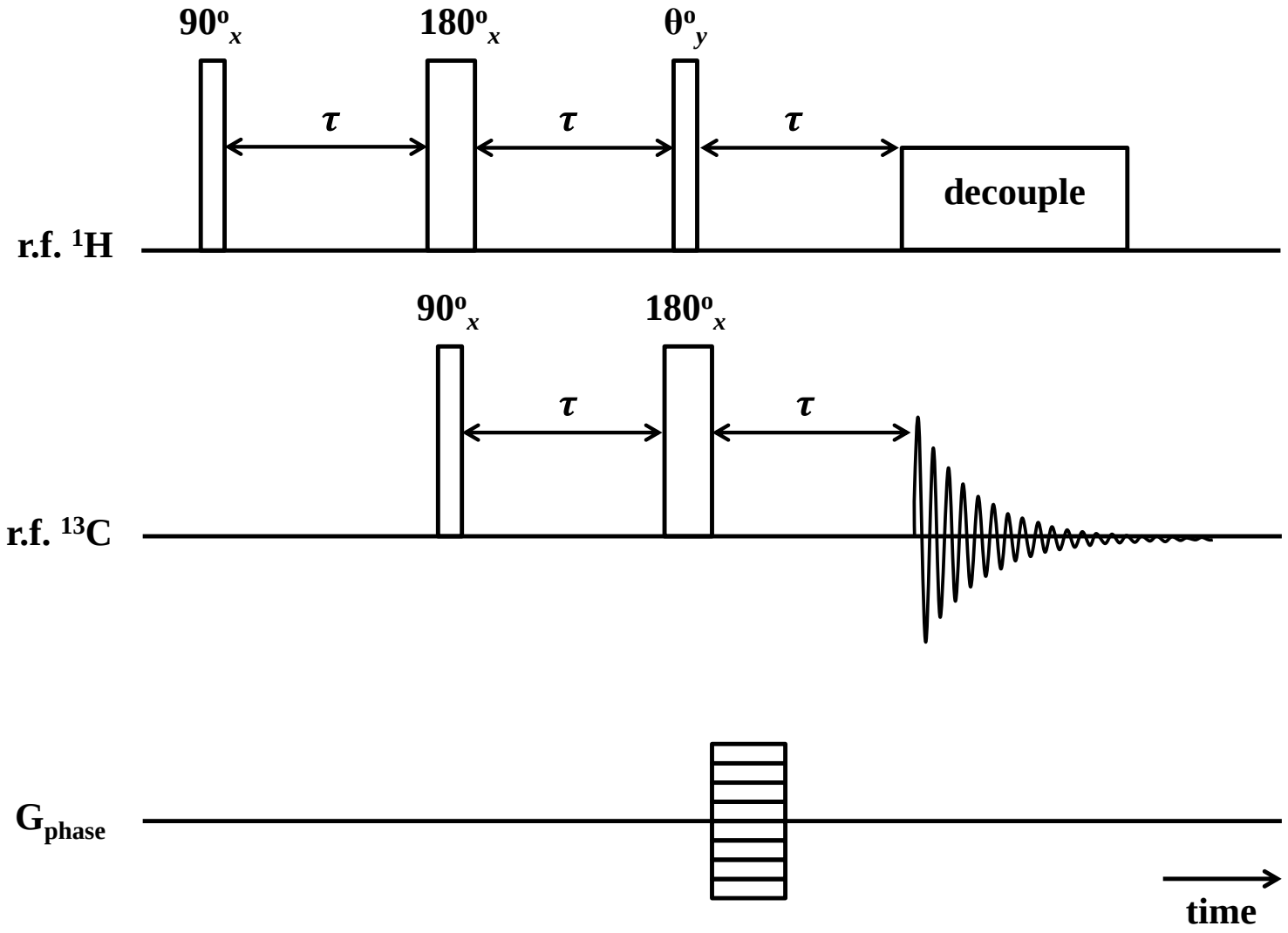

Figure 2

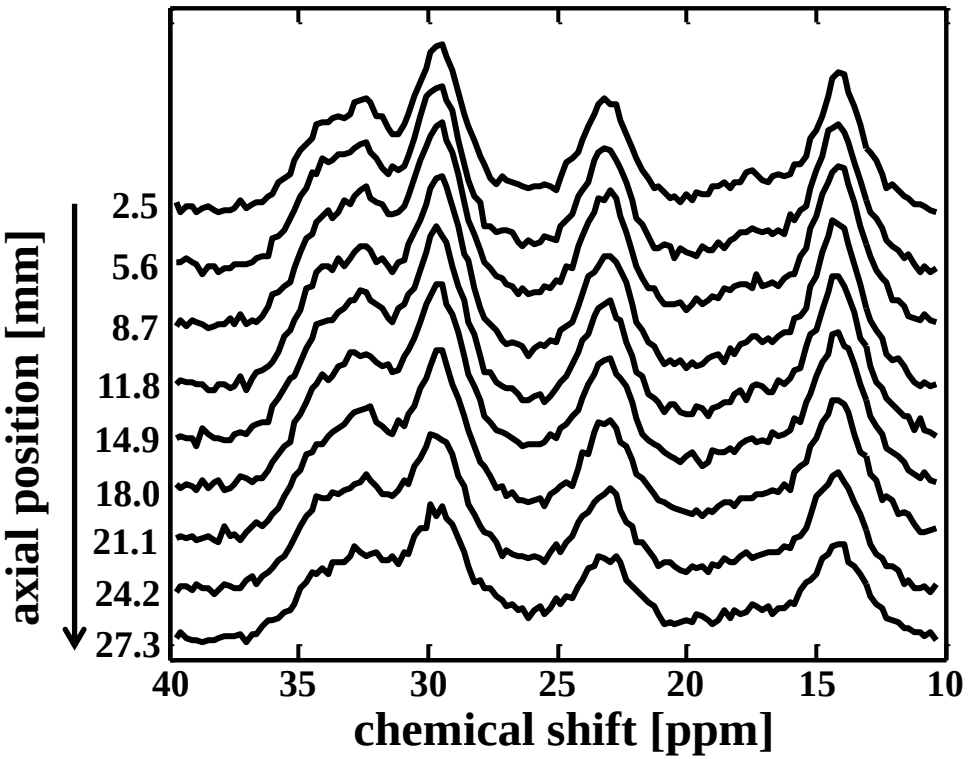
axial position [mm]
2.5
5.6
8.7
11.8
14.9
18.0
21.1
24.2
27.3
40
35
30
25
20
15
10
chemical shift [ppm]

Figure 3

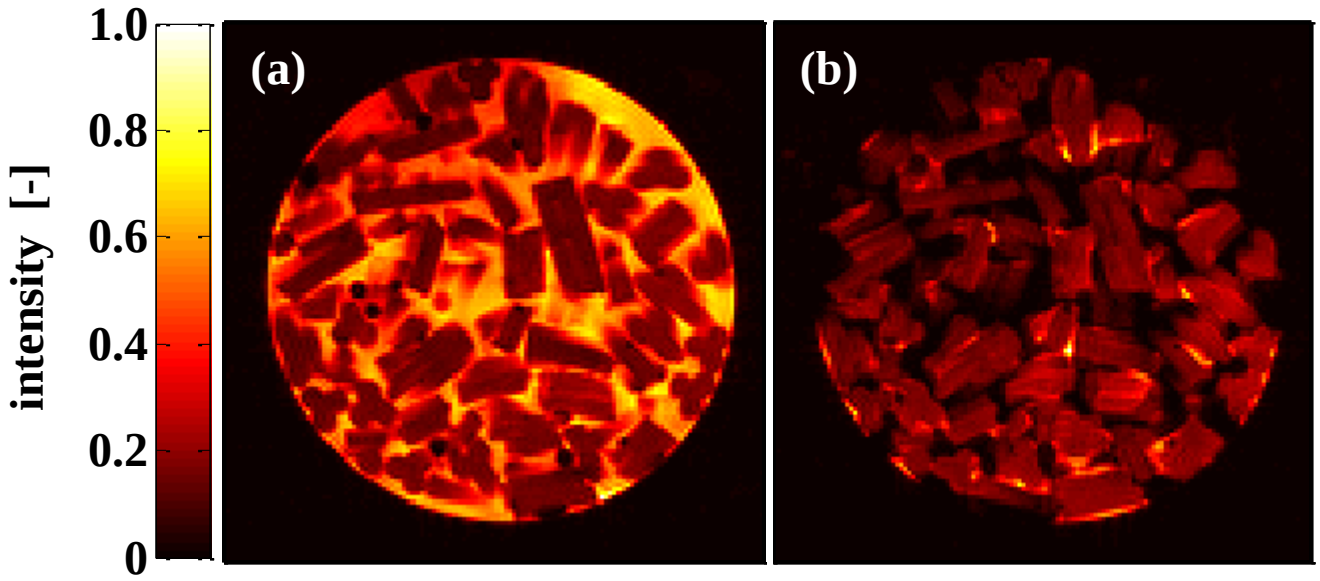

Figure 4

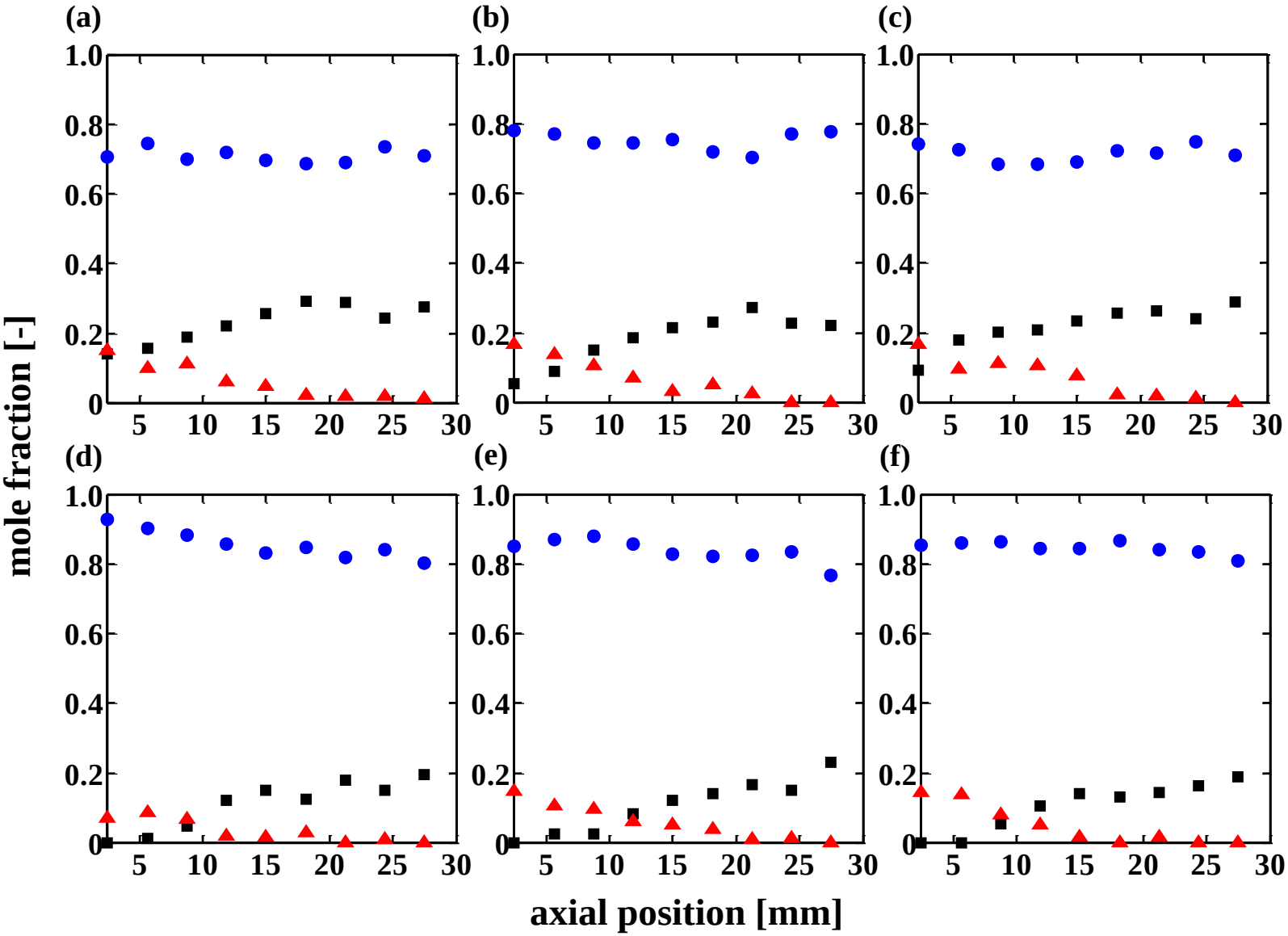
(a)
(b)
(c)
(d)
(e)
(f)
mole fraction [-]
axial position [mm]
0
0.2
0.4
0.6
0.8
1.0
5
10
15
20
25
30

Figure 5

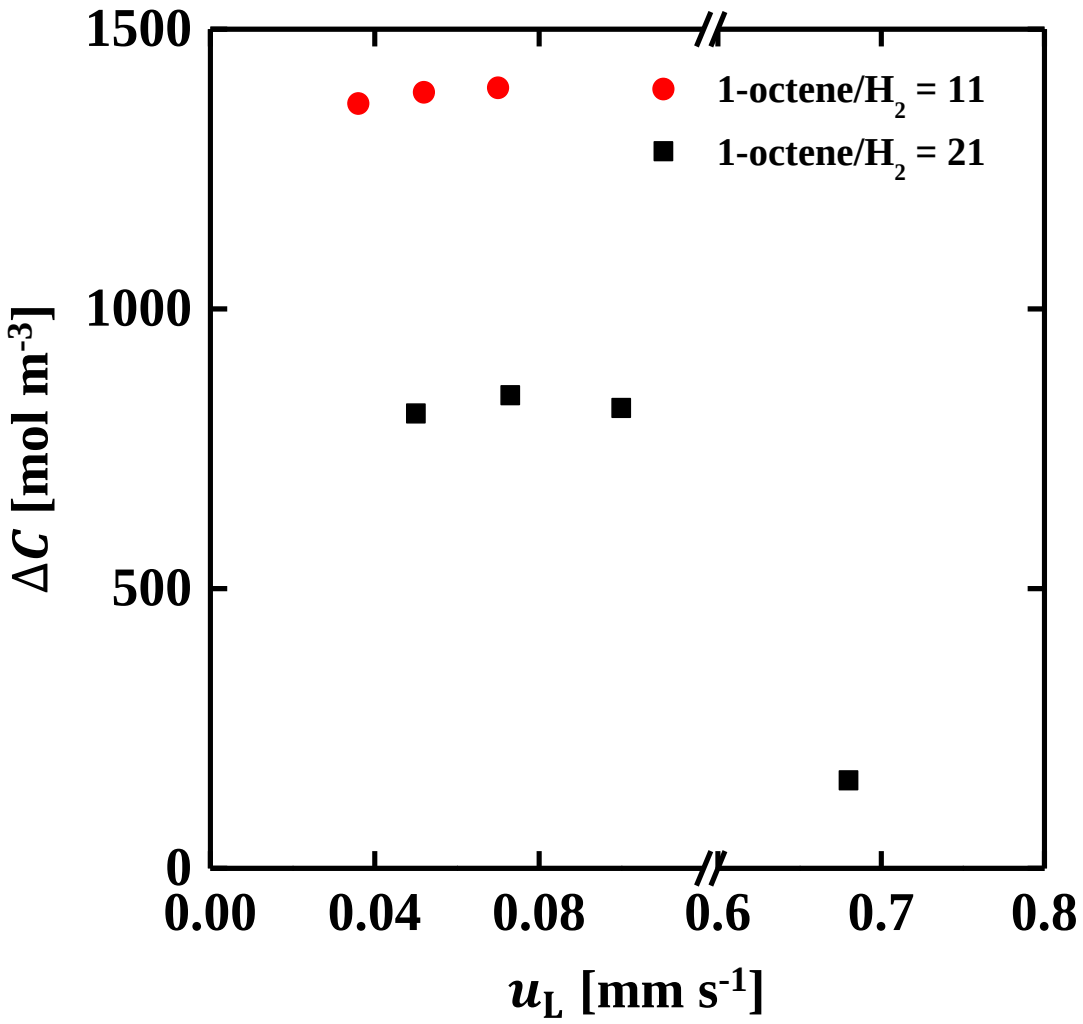
1500
1000
500
0
ΔC [mol m-3]
0.00
0.04
0.08
0.6
0.7
0.8
uL [mm s-1]
1-octene/H2 = 11
1-octene/H2 = 21

Figure 6

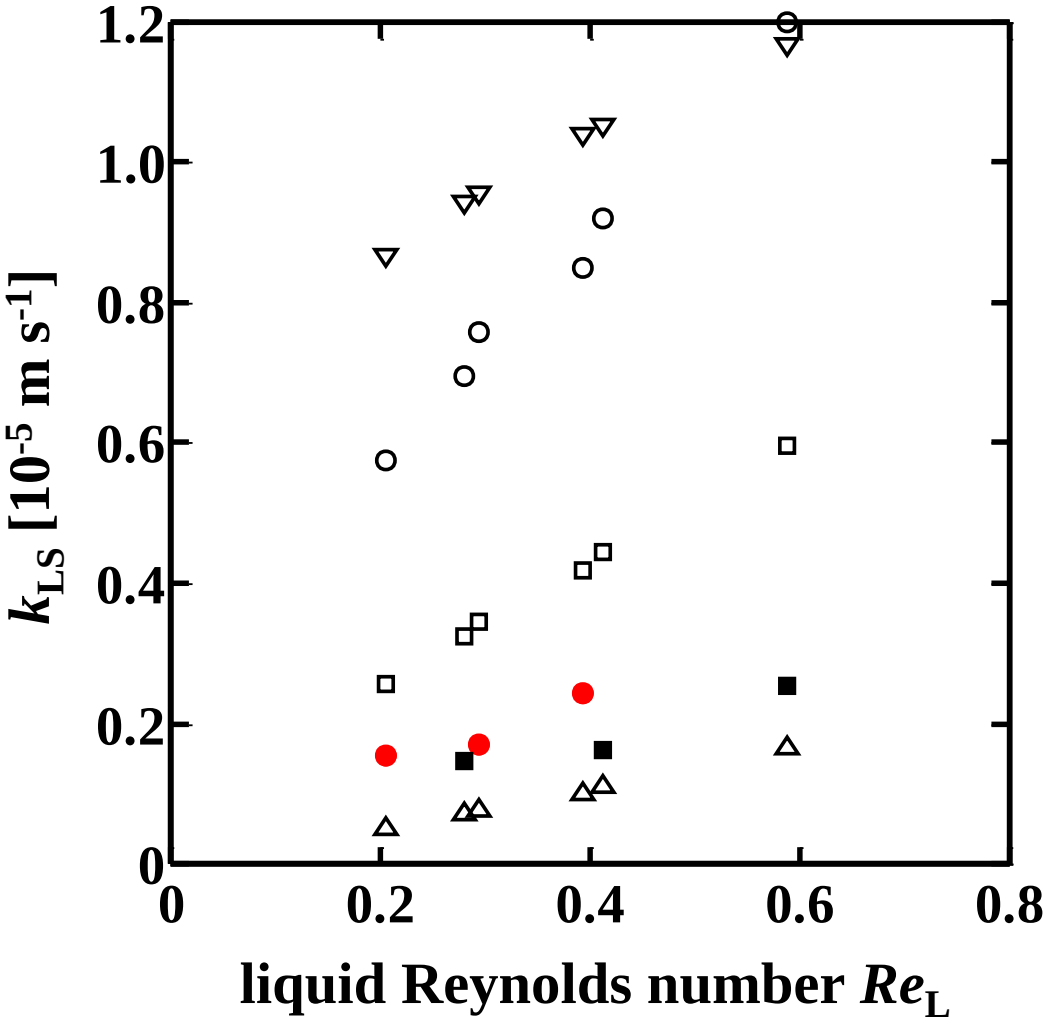
1.2
1.0
0.8
0.6
0.4
0.2
0
0
0.2
0.4
0.6
0.8
k_{LS} [10^{-5} m s^{-1}]
liquid Reynolds number Re_L

Figure 7